Electron-impact cross sections for multiple ionization of Kr and Xe

Jack A. Syage

The Aerospace Corporation, P.O. Box 92957/M5-754, Los Angeles, California 90009

(Received 9 August 1991; revised manuscript received 18 May 1992)

Partial cross sections were measured for the ionization $M + e \rightarrow M^{n+} + (n+1)e$ for $M = $ Kr and Xe ($n = 1$–6) as a function of electron energy (0–470 eV). The experiment is based on a crossed-beam time-of-flight mass spectrometer employing pulsed electron and atomic beams, and pulsed ion extraction. Cross sections for Kr^{5+}, Kr^{6+}, and Xe^{6+} have not been previously measured over this energy range. The cross sections reported for the remaining ions considerably narrow the uncertainty of previous measurements. The source of discrepancy among recent work appears to be due to improper account of detector-gain effects. The ionization onsets are fitted to threshold power-law expressions to derive ionization potentials.

PACS number(s): 34.80.Dp, 35.10.Hn

I. INTRODUCTION

Collisions involving electrons with atoms and molecules are one of the most fundamental interactions in physics. These events are basic to a variety of processes such as plasma physics (discharges and breakdowns, fusion, bremsstrahlung processes), radiation physics (secondary-electron effects, condensed-phase spur formations), and astrophysics (aurora borealis, planetary atmospheres, supernova activity). Electron-impact (EI) is also the most common form of ionization in commercial mass spectrometers and is used as an analytical tool for measuring species concentrations in gaseous samples. Yet reliable measurements of EI ionization cross sections are lacking except for the simplest atoms and molecules. The literature abounds with comparisons of cross-section measurements by different techniques [1–13]. Cross sections for single ionization of the rare gases are generally regarded as well known with independent measurements now agreeing to within 5–10 % [3–7]. Recent measurements of multiple-ionization cross sections, in contrast, exhibit serious discrepancies.

We use an approach for measuring energy-dependent EI-ionization cross sections based on crossed electron and atomic (or molecular) beams and a time-of-flight mass spectrometer [12,13]. The apparatus employs (1) pulsed beam sources, (2) a field-free ionization volume, (3) two-stage high-voltage ion extraction, and (4) multichannel mass detection. These features account for high ion transmission, a large detector field of view, and a relative immunity to the usual mass-to-charge ratio (m/z) and kinetic-energy-discrimination effects. The accuracy of making cross-section measurements was demonstrated in a preliminary account of this technique [12]. Additional experimental enhancements have been made in this work to improve accuracy. In particular, special attention is given to the problem of detector gain variations with ion impact energy, which can seriously impair the measurement of multiple-ionization cross sections even when using pulse-counting methods [13].

We report on the electron-impact cross sections for multiple ionization of Kr and Xe. Multiple ionization of rare gases has been a subject of interest for many years [3–7,14–22]. Tate and Smith measured ionization thresholds and rough energy-dependent curves for ion charges as high as Kr^{4+} and Xe^{6+} [15]. Fox reported ionization thresholds up to Kr^{6+} [16]. Stuber followed with measurements of Kr^{n+} and Xe^{n+} up to $n = 8$ and 9, respectively [17]. The latter two investigators compared the energy dependence near threshold to simple threshold laws for n-fold ionization [23]. They also presented energy-dependent intensities at higher energies that for certain ions showed structure in the form of discontinuities and multiple maxima. However, instrumental effects precluded making cross-section measurements. Also, the shape of the ionization efficiency curves and the relative intensities between ions of different charge are not in good agreement with more recent measurements [3–7]. Dorman, Morrison, and Nicholson reported on the threshold regions for Xe^{n+} up to $n = 6$ [18]. Other investigators concentrated on high-energy excitation (to several keV) [20–22]. Since energy resolution was not a major concern in these experiment, a large extraction field was applied across the ionization volume to obtain high collection efficiency. This eliminated the problem of ion transmission, but did not remove all discrimination effects, judging by the large discrepancies that exist in the reported cross sections. The most serious effect now appears to be detector-gain dependence on ion impact energy. Known to be a problem in current mode, we show that it also can corrupt measurements that use pulse counting [13].

The most reliable and extensive set of energy-dependent cross-section measurements to date for Kr and Xe are by Stephan, Helm, and Märk (SHM) [3,4], Wetzel, Baiocchi, Hayes, and Freund (WBHF) [5], and Krishakumar and Srivastava (KS) [6]. The measurements by SHM and WBHF are in reasonable agreement where their data overlap (Kr^{n+} and Xe^{n+}, $n = 1$–3, $E = 0$–180 eV). The work of KS has extended the range of cross-section data to energies of 1000 eV and to charges as high as Kr^{4+} and Xe^{5+} (as well as Ne^{3+} and Ar^{3+}). The shape of their

cross section curves agrees well with SHM and WBHF. However, the absolute values are invariably larger and the discrepancy increases with ion charge (reaching a factor of 2 for Kr^{4+}). Further complicating the comparison are the cross-section results of Ma, Spoleder, and Bonham (MSB) [7] for multiple ionization of Ar, which are much closer in magnitude to the results of KS than to SHM and WBHF.

The present investigation reports partial cross sections [24] for the ionization $M + e \rightarrow M^{n+} + (n+1)e$ for $M = Kr$ and Xe ($n = 1-6$) over the electron energy range 0–470 eV. These results include measurements that overlap with those of SHM [3,4], WBHF [5], and KS [6], which we present in an attempt to resolve the source of discrepancy that exists among these and other data on multiple ionization. We have identified a systematic detector-gain effect that may explain the discrepancy [13]. Our results support the absolute magnitudes reported by SHM and WBHF. These measurements also extend to higher energy and ion charge than previously reported and provide more accurate values in the threshold regions. The cross sections for ionization to Kr^{5+}, Kr^{6+}, and Xe^{6+} have not been previously measured over the energy range reported here.

II. EXPERIMENTAL DETAILS

A. Apparatus

A preliminary account of the apparatus as used for EI cross-section measurements has been reported before [12,13]. A description of the apparatus as used for more general studies (e.g., multiphoton-ionization, spectroscopy, and picosecond time-domain measurements) is given in other publications [25–27]. An experimental schematic relevant to the present work is given in Fig. 1.

1. Molecular beam

The vacuum system consists of a differentially pumped source and ionization chamber [26]. The source chamber contains a temperature-controlled solenoid-actuated

FIG. 1. Geometry and configuration of the crossed electron-atomic beams and the time-of-flight mass spectrometer. Components and operation are described in the text. The schematic is not drawn to scale.

pulsed nozzle, which is used to produce a supersonic jet expansion (Fig. 1). The narrow velocity distribution of the jet assists in achieving maximum ion detection efficiency. Typical expansion conditions are 10-psi (absolute) sample pressure, 500-μm nozzle diam, 2-cm nozzle-skimmer distance, and 400-μs pulse width. The atomic beam enters the ionization chamber through a 1-mm-diam skimmer. The beam divergence is about 0.04 mrad and the beam diameter about 4 mm at the excitation region. The pulsed expansion accounts for high density at the excitation volume ($> 10^{13}$ atoms/cm^3) and low ambient pressure in the ionization chamber [typically $(1-2) \times 10^{-8}$ Torr, rising to $(2-5) \times 10^{-7}$ Torr or about 10^9 atoms/cm^3 at 50-Hz operation].

2. Ionizer and time-of-flight mass spectrometer

The pulsed EI ion source and time-of-flight (TOF) ion optics configuration is illustrated in Fig. 1. The spacing between adjacent grids labeled $V0$ to $V3$ is 1 cm. The atomic beam traverses the region between grids $V1$ and $V2$. The drift-tube length is 100 cm and the detector is a dual microchannel plate (MCP) with a 18-mm-diam active area and a 50-Ω coaxial cone anode. In the following discussion we use the terms $V0 - V4$ to designate both the ion-optics components and the bias voltage applied to them.

The electron source is based on the design by Pollard and Cohen [28]. The voltage $V4$ applied to the filament determines the electron energy E that impinges on the atomic beam. (The shield can is maintained at the filament potential.) The electrons are prevented from exiting the source by grid $V3$, which is maintained at a lower potential than the filament $V4$ (using a 30-V Zener diode). An electron beam pulse is admitted to the field-free excitation region by applying a 40-V gate pulse $P3$ of duration 50–500 ns to $V3$. The electron beam is collimated to a diameter of approximately 5 mm by the apertures at $V2$ and $V3$. This ensures complete overlap with the atomic beam. The electron flux during the pulse period (expressed as peak current) was varied from 0.01–1.0 μA for pulse counting and typically less than 10 μA for current measurements. Further details on the electron source are given in Sec. II A 3. Electron energies are scanned by stepping the voltage to plate $V3$ and filament $V4$. A 0–10-V control signal is generated from a 80286-type computer and 12-bit digital-to-analog (D/A) general-purpose interface board (GPIB), which externally controls the power supply. Our previous work employed a scanning high-voltage (3-kV) power supply, thus limiting the electron energy step size to a minimum of 1 eV [12]. We now float the high voltage power supply (set at fixed voltage) using a computer-scanned 0–250-V power supply. This permits a scanning resolution of 60 meV.

The excitation region is maintained field-free during ionization. A base potential is applied to $V1$ (typically 1500 V). The potential at $V2$ is adjusted relative to $V1$ with a ten-turn potentiometer in a voltage-divider network to compensate for field penetration at $V1$ induced by $V0$ at ground potential. A procedure for ensuring the absence of residual fields is described in Sec. II B 5. The
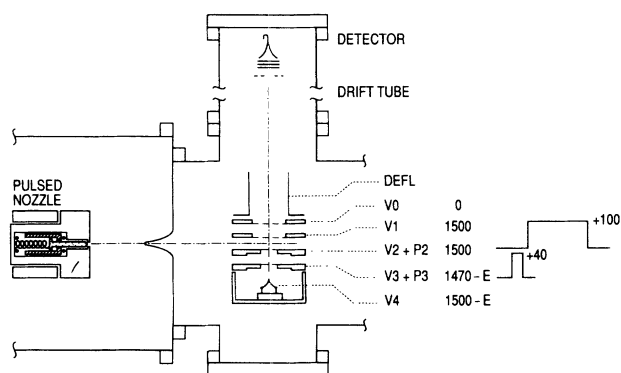
ions that are formed are extracted out of the ionization region by a 100-V, 4–6-μs repeller pulse $P2$ applied to $V2$. The ions are further accelerated in the $V0$-$V1$ region to a final energy of 1650 eV (for singly charged ions) before entering the field-free drift tube leading to the detector. Deflector plates (DEFL) are used to compensate for the atomic beam velocity orthogonal to the drift tube axis.

The signal at the detector anode is collected by charge integration (current mode) or pulse counting over gate periods spanning the distribution of TOF's for each ion (Fig. 2). Because of the high density of the atomic-beam pulses, low repetition rate of the experiment (50 Hz), and narrow TOF distributions of the ion signal, better signal-to-noise ratio is obtained by current detection than by pulse counting. This mode is used to record ion yield versus electron energy. Ion production rates of approximately 10^5 s^{-1} and MCP gain of 10^6–10^7 are adjusted to limit anode current to less than 1% of strip current, thus ensuring linearity. The signal is collected by a gated boxcar averager, digitized by a 12-bit A/D converter, and passed to the computer over the GPIB interface. A data-acquisition computer program allows repetitive scans as well as adjustable dwell times between electron energy increments.

Pulse counting is used to avoid the problem of detector-gain dependence on mass-to-charge ratio m/z [13]. In counting mode, the MCP detector is operated at 10^7 gain (1 kV/plate) and the anode pulses amplified by $\times 40$ and filtered by a 20-ns time constant (the latter to eliminate spurious counts due to ringing). The TOF distributions (Fig. 2) are broad enough relative to the individual pulse widths of 25–30 ns to reduce the problem of
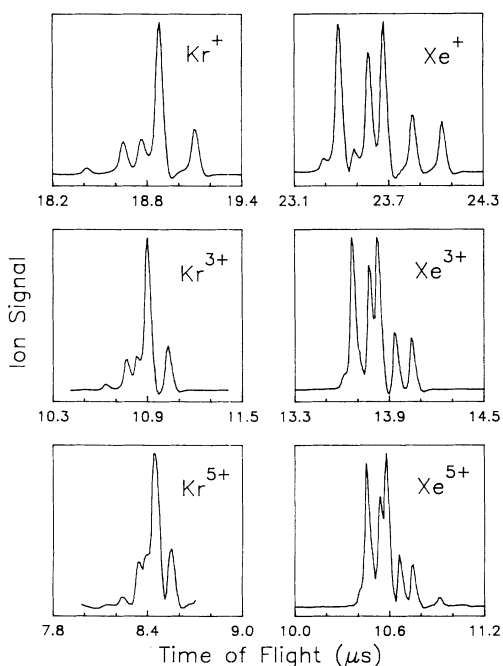
multiple hits (the isotope distribution of Kr and Xe help here). Nonetheless total count rates were not allowed to exceed 5 s^{-1} (2 s^{-1} typical) at 50-Hz repetition rate. The frequency of double strikes is carefully monitored and small corrections are made when necessary to compensate for under counting. Discriminator levels were set to detect essentially all ion pulses within this gate period (Sec. II B 3). Background counts in the absence of the atomic beam were less than 10^{-3} times the typical signal. By pulse counting for long periods of time at a few energies, reliable cross section ratios were obtained for scaling the energy-dependence curves measured in current mode.

TOF mass spectra are recorded using a 100-MHz digital oscilloscope. Mass resolution is not critical in these experiments because the ions of interest are well separated from each other. Resolution of $m/\Delta m > 300$ is easily achieved, however, for weak signals and for pulse counting it is preferable to operate toward gain-saturation conditions, which broadens the arrival time distribution to $m/\Delta m \leq 200$ for singly charged ions and less for multiply charged ions. Plots of arrival time distributions for Kr^{n+} and Xe^{n+} isotopes are given in Fig. 2.

3. Electron-beam characteristics

The electron-beam source is an unconventional design in that it is aligned along the TOF axis and therefore is not terminated by a Faraday cup. This arrangement was chosen to make available an axis for laser excitation that is orthogonal to the molecular (atomic) beam and electron beam (as well as orthogonal to the TOF axis). Crossed electron–laser–molecular-beam experiments have been carried out using this apparatus [25]. Below we describe the characteristics of our electron-beam source in terms of the energy resolution and the extent to which the uncollected electron beam adversely affects our measurements.

The electron beam crosses the atomic beam in the field-free region between grids $V2$ and $V1$ whereupon it enters the region between $V1$ and $V0$ and encounters a 1500-V/cm reflecting field. The electron beam makes a return pass through the atomic beam and continues toward $V3$ where it slows to 10 eV ($V3+P3-V4$). The least diverged central part of the beam can pass through the aperture at $V3$. However, the vast majority of the beam disperses or strikes the $V3$ surface and is conducted or scattered away. A small fraction of electrons can also scatter off the grid at $V1$ or the aperture at $V2$. All of these events occur within the $P3$ electron gate pulse period. A number of issues may be raised regarding the electron-beam source. These include (1) the narrowness of the electron energy distribution at the atomic-beam intersection, (2) whether the dispersed and scattered electrons cause unwanted ionization that interferes with the desired signal, and (3) whether scattering of electrons off surfaces desorbs ions that interfere with the desired signal. None of these concerns are important in our experiment as explained below.

The electron beam traverses the atomic beam under field-free conditions during the initial and reflected pass; therefore in the absence of scattering collisions the

FIG. 2. TOF distributions for multiply charged ions Kr^{n+} and Xe^{n+}.

electron-beam energy distribution is expected to be space-charge limited (i.e., $\Delta E < 1$ eV). The probability of electron-energy-changing collisions with gas molecules is minimal for the density n and pathlength l of the atomic beam $(nl \sim 10^{13}$ atoms/cm$^2)$ and background gas $(nl < 10^{10}$ atoms/cm$^2)$. Several tests and measurements indicate an energy resolution of about 2 eV, sufficient for these studies. For example, the observed curvature for threshold ionization is a convolution of the natural threshold curvature and the electron energy distribution. We measured a threshold width for Ar$^+$ from the rate of change of intensity with energy (i.e., dI/IdE) of 3 eV and a second derivative width of 1 eV. Electron energy distributions were also measured by reconfining our ion optics for retarding field measurements and by time resolving the spread of the electron-beam pulse transmitted to the detector. A tailing on the low-energy side of the distribution (affecting less than 10% of the electrons) was observed, possibly due to scattering off of grid $V2$.

The most serious source of undesirable signal in terms of intensity and proximity in time to the mass of interest occurs by ionization of background gas by the primary electron beam during its reflected trajectory above grid $V1$. Ions formed in this region are immediately accelerated toward the detector. However, they are readily detected in a TOF mass spectrum as a broad signal that appears before the narrow (space-focused) atomic-beam ionization signal. The background signal is greatest in the absence of deflection voltage (typically about 5% of the desired signal), but essentially disappears at the deflection voltages that optimize the detection of atomic-beam ions. Dispersed or scattered electrons can conceivably ionize background gas; however, this contribution is considerably less than background ionization by the primary electron beam. Furthermore, ions that reach the detector are not correlated in time with the signal of interest.

Finally, the probability that ions, desorbed from surfaces by electron scattering, appear in the time gate for detection of a particular ion is negligible. Ions of different mass are identifiable by their TOF's. Ions formed over large spatial extents will also have broad signals that are readily detected. The mass spectra observed in our experiments consist only of narrow ion signals due to atomic-beam ionization. Time-of-flight mass spectrometry has the valuable advantage over other forms of mass spectrometry in that it is a time-correlated technique and therefore has excellent immunity to background interference.

4. Sample preparation

A reference sample consisting of calibrated quantities of the five rare gases (prepared by Matheson) is used to obtain cross section ratios with the ion of interest. The energy-dependent cross sections for single ionization of Kr and Xe is obtained by referencing to the known cross sections for Ar ionization (described below). Cross sections for multiple ionization are obtained using pure samples of Kr and Xe and referencing the multiply charged ions to the singly charged ion cross sections previously

determined. Formation of clusters in the supersonic expansion could be observed in low-energy EI mass spectra. Clustering was effectively suppressed by operating at low backing pressure [6–15 psi (absolute)] and employing a heated nozzle (60–100 °C).

B. Procedure and calibration

1. Cross-section determination

Ionization cross sections as a function of electron energy E are obtained by measuring the ion yield of target species M relative to a well-established reference species R according to the equation

$$\sigma_M(E) = \frac{I_M n_R}{I_R n_M} \sigma_R(E) \kappa_{M,R} , \tag{1}$$

where σ is cross section, I is ion signal intensity, and n is number density. The function $\kappa_{M,R}$ encompasses instrumental effects that may give rise to different detection efficiencies for M and R. The ratio n_R/n_M is obtained by preparing a sample containing calibrated quantities of M and R. The cross sections for single ionization of Kr and Xe were measured by referencing to Ar. The values of σ_{Kr^+} and σ_{Xe^+}, after confirming their reliability against previous measurements [3–6], were then used as the reference for determining the cross sections for multiple ionization.

We have compiled a reference data set of cross sections $\sigma_R(E)$ for the internal standard Ar$^+$ by averaging the measurements of SHM [3,4], WBHF [5], KS[6], and MSB [7] as described previously [13]. Only the latter two results extend beyond 200 eV. All results agree to within 5–10 % of the average except for the values of KS near threshold, which are significantly lower; hence the values for ≤ 25 eV were excluded from the average. As a consistency check, we find that the cross section ratio $\sigma(300$ eV$)/\sigma(150$ eV$)$ of 0.723 for the reference set is in good agreement with Crowe, Preston, and McConkey (0.73) [9], Stuber (0.76) [17], and Bleakney (0.76) [14]; and the value $\sigma(470$ eV$)/\sigma(150$ eV$)$ of 0.554 agrees well with Stuber (0.53) [17] and Bleakney (0.57) [14]. We list the Ar$^+$ reference data set in Table I to make it possible to recalculate cross sections using Eq. (1) should better Ar$^+$ data become available. Polynomial (fourth-order) linear regressions were fitted over small regions of the σ_{Ar^+} data base to interpolate σ_R to any value of E. Our cross-section measurements for Ar^{n+} from a previous report [13] are also tabulated in Table I.

The present method eliminates many of the shortcomings of more conventional techniques [1,2], as discussed previously [12]. Problems with ion extraction efficiency are avoided by using pulsed extraction (100 V, 4 μs) and acceleration (1500 V) following field-free ionization. TOF mass spectrometry permits simultaneous detection of more than one ion signal making the intensity ratio measurement in Eq. (1) very reliable. The need to fully characterize the electron-beam properties (flux, divergence, interaction length, dependence on energy) is, therefore, eliminated. The instrumental effects having

m/z dependencies that remain in our experiment are due to deflection voltage, MCP detector gain, and lack of uniformity of the relative number density n_R/n_M in the molecular beam. We express the instrument function $\kappa_{M,R}$ in Eq. (1) in terms of these three contributions, respectively, by

$$\kappa_{M,R} = \Gamma_{\text{defl}}\Gamma_{\text{det}}\Gamma_{\text{nrel}} . \tag{2}$$

These factors are each described below.

2. Deflection function

Because the atomic beam travels orthogonal to the TOF drift tube axis, a deflection potential is applied to the ion trajectories to offset the forward velocity of the beam. The optimum deflection voltage for maximizing ion signal varies with m/z because of the different ion arrival times at the detector (increasing values of m/z require increasing deflection voltage).

The single-ionization cross sections for Kr and Xe (using Ar as the reference) were measured using a sample containing calibrated quantities of the five rare gases diluted in He. The deflection response is sensitive to m/z as seen in Fig. 3(a) for Ar^+, Kr^+, and Xe^+. The relatively flat peak intensities reflect the ion packet sweeping across the detector surface and is evidence that nearly all ions are striking the detector. The Γ_{defl} values in Fig. 3(b)

TABLE I. Partial cross sections for electron-impact ionization to multiply charged ions of Ar (1 Mb = 10^{-18} cm^2). [a]The single-ionization cross sections represent the reference data set compiled from literature values as described in the text. Measured values for $n = 2-5$ are from Ref. [13]. Error limits are discussed in Sec. II B 6.

| E (eV)	σ (10^{-18} cm^2)					E (eV)	σ(10^{-18} cm^2)				
	Ar^+ [a]	Ar^{2+}	Ar^{3+}	Ar^{4+}	Ar^{5+}		Ar^+ [a]	Ar^{2+}	Ar^{3+}	Ar^{4+}	Ar^{5+}
18	29.3					260	188	10.9	0.41	0.008	0.0002
20	58.4					270	184	10.7	0.41	0.009	0.0002
22	83.3					280	180	10.4	0.38	0.011	0.0003
24	110					290	176	10.1	0.40	0.013	0.0003
26	134	0.01				300	172	9.78	0.42	0.014	0.0003
28	155	0.04				310	168	9.51	0.40	0.016	0.0004
30	175	0.03				320	165	9.28	0.42	0.019	0.0005
32	191	0.07				330	162	8.97	0.44	0.021	0.0005
34	206	0.10				340	159	8.81	0.45	0.024	0.0007
36	218	0.15				350	156	8.55	0.49	0.028	0.0009
38	228	0.16				360	153	8.33	0.48	0.031	0.0012
40	236	0.24				370	151	8.13	0.50	0.033	0.0013
42	242	0.32				380	148	7.92	0.50	0.036	0.0016
44	247	0.51				390	146	7.72	0.51	0.039	0.0018
46	250	0.78				400	144	7.60	0.50	0.043	0.0019
48	252	1.17				410	142	7.40	0.53	0.046	0.0022
50	253	1.42				420	140	7.29	0.53	0.048	0.0026
52	254	2.93				430	138	7.12	0.54	0.050	0.0028
56	253	4.32				440	136	7.00	0.54	0.054	0.0030
60	253	5.67				450	135	6.92	0.52	0.055	0.0032
64	252	6.94				460	133	6.72	0.54	0.060	0.0033
68	253	8.23				470	132	6.70	0.55	0.062	0.0033
72	254	9.68				480	130	6.53	0.56	0.064	0.0036
76	255	11.0				490	128	6.45	0.54	0.066	0.0038
80	257	12.3				500	127	6.34	0.55	0.068	0.0038
84	257	13.4				510	125	6.23	0.54	0.069	0.0044
88	256	14.1				520	124	6.13	0.54	0.070	0.0051
92	255	14.7	0.01			530	122	6.03	0.54	0.076	0.0048
96	254	15.4	0.02			540	121	5.96	0.55	0.076	0.0052
100	253	15.8	0.04			550	120	5.86	0.55	0.078	0.0054
110	252	16.1	0.09			560	118	5.72	0.56	0.079	0.0055
120	249	16.3	0.17			570	117	5.65	0.56	0.076	0.0066
130	245	16.2	0.24			580	116	5.60	0.55	0.080	0.0054
140	242	16.1	0.32			590	115	5.51	0.54	0.082	0.0058
150	238	15.7	0.37			600	113	5.44	0.55	0.084	0.0064
160	234	15.3	0.41			610	112	5.38	0.56	0.083	0.0059
170	229	14.9	0.44	0.001		620	111	5.32	0.56	0.084	0.0060
180	225	14.4	0.46	0.001		630	110	5.22	0.56	0.085	0.0064
190	220	13.9	0.44	0.002		640	109	5.18	0.55	0.087	0.0066
200	215	13.5	0.45	0.002		650	108	5.10	0.55	0.088	0.0071
210	211	13.0	0.44	0.003		660	107	5.06	0.55	0.089	0.0075
240	197	11.7	0.43	0.005							
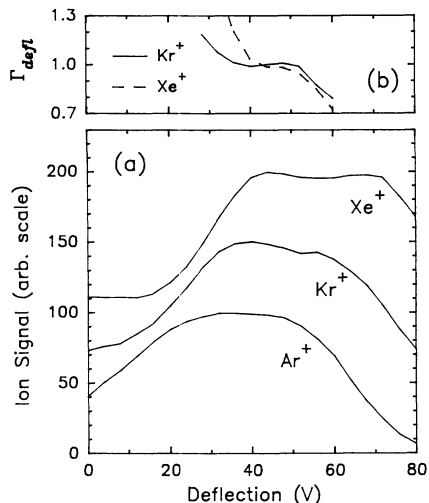
FIG. 3. (a) Measured deflection functions for Ar^+, Kr^+, and Xe^+ representing ion-signal strength vs deflection voltage. All curves are normalized to a 0–100 scale and offset by 50 units for clarity. (b) The intensity ratio f^R_{defl}/f^M_{defl}, where $R = Ar$ and $M = Kr, Xe$, constitutes the correction factor Γ_{defl} in Eq. (2).

are obtained from the ratio of deflection efficiencies f^R_{defl}/f^M_{defl} from Fig. 3(a) (where f is the fraction of the maximum intensity). A deflection voltage of 40 V was chosen for these experiments because it is near the response peak for all three ions and minimizes the deviation of Γ_{defl} from unity [0.987 and 1.033 for Kr^+ and Xe^+, respectively, from Fig. 3(b)].

Cross sections for multiple ionization of Kr and Xe were measured using pure gas samples and referencing to single-ionization cross sections. The slower beam velocity for these heavier atoms gives rise to deflection responses that are relatively insensitive to m/z as shown in Fig. 4 for Xe. Kr gives a similar response except shifted slightly
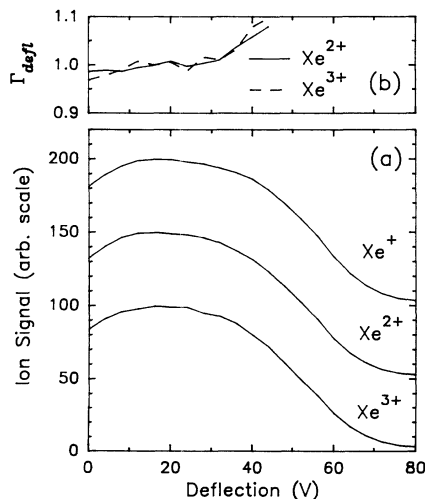

FIG. 4. (a) Measured deflection functions for Xe^+, Xe^{2+}, and Xe^{3+}. (b) Intensity ratio f^R_{defl}/f^M_{defl} is for $R = Xe^+$ and $M = Xe^{2+}$ and Xe^{3+}.

to lower voltage. Deflection voltages of 25 and 30 V were used for Kr and Xe, respectively, corresponding to Γ_{defl} factors of 1.011 (Kr^{2+}), 0.988 (Kr^{3+}), and 1.007 (Xe^{2+}), 1.014 (Xe^{3+}) [Fig. 4(b)] (we assume 1.0 for the higher charged ions). Clearly the deflection function is an instrumental effect of minor consequence to these experiments.

3. Detector-gain effects

The gain of an electron multiplier detector varies with the mass and velocity of the impacting ion [13,29–31]. In an acceleration field, ions of greater charge reach proportionately greater kinetic energy. As impact energy increases, the detector surface expels a greater number of secondary electrons. This causes an increase in gain. The m/z discrimination effect of electron multipliers is most problematic when measuring charge or current at the detector anode. Current mode has superior signal-to-noise in these experiments and is used to record the energy dependence of the cross sections for each m/z. However, pulse counting is used to record the relative intensities for different values of z. Measurements at several electron energies were collected and used to normalize the energy-dependent curves. These determinations also establish that the pulse count versus anode current intensities are linear. A comparison of the relative intensities for different ion charges measured by current mode and by pulse counting permits the relative gain of the detector to be determined. The results for Kr^{n+} and Xe^{n+} are plotted in Fig. 5.

Pulse counting is also subject to detector m/z effects because pulse height distributions (PHD's) depend on gain which varies with ion charge. The ions are accelerated toward the MCP by a 1.55-kV potential and the front surface of the MCP is biased at -2.2 kV. The ion impact energies are, therefore, given by $n \times (1.55 + 2.2)$ keV. The measured PHD's for Kr^+, Kr^{3+}, and Kr^{5+} in Fig. 6 clearly show an increase in detector gain with ion-impact energy. It is important for reliable pulse counting of multiply charged ions that a minimal discrimination level be employed. Discrepancies in previous multiple-
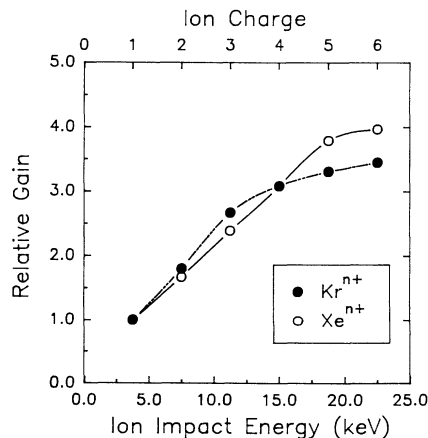

FIG. 5. MCP gain for Kr^{n+} and Xe^{n+} as a function of ion impact energy and corresponding ion charge.
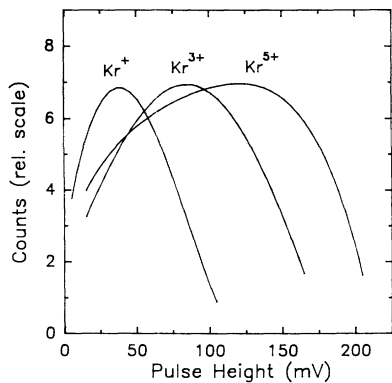
FIG. 6. Pulse-height distributions for detection of Kr^+, Kr^{3+}, and Kr^{5+} produced by 370-eV excitation. Measurements are for amplified and filtered ion pulse shapes (Sec. II A 2). Counts were measured over 5-mV channels. Curves are drawn through points for easier viewing and are normalized to the same maximum value.

ionization cross-section measurements are believed to be due in part to unanticipated variations of PHD's with ion charge (cf. Sec. III A). Operating close to gain saturation conditions reduces the problem because the PHD is narrower and the discriminator setting less critical. A single-channel multiplier (e.g., channeltron) is preferable to a dual MCP in this regard.

4. Relative number density in atomic beam

The validity of using Eq. (1) to obtain absolute cross sections depends on the premixed ratio n_R/n_M remaining uniform in the molecular beam expansion. The correction factor Γ_{nrel} represents the ratio of n_R/n_M at the excitation region to that in the premixed sample. The value n_R/n_M in the molecular beam is likely to deviate from the premixed sample because the radial velocity is mass dependent, which causes an increased concentration of heavier masses along the beam centerline (i.e., mass focusing) [32].

These problems are avoided in this experiment. Mass-focusing affects the absolute value, but not the shape of cross-section curves with energy. We therefore recorded cross-section curves for Kr^+ and Xe^+ referenced to the Ar^+ data base, but normalized the curves to absolute cross section data for Kr^+ and Xe^+ obtained from the average of the SHM and WBHF values at 70 eV. The normalization changes the magnitude of the recorded curves only slightly corresponding to Γ_{nrel} values of Eq. (1) of 0.932 and 0.875 for Kr and Xe, respectively. Mass focusing in the molecular beam is not a concern when measuring multiple-charge cross sections because the target and reference ions (e.g., Kr^{n+} relative to Kr^+) originate from the same neutral atom.

5. Energy calibration

The $V0$ ground grid causes field penetration through the $V1$ grid (we use 70 lines/in., 90% transmitting grids), which degrades the field-free region between grids $V1$

and $V2$. This penetration is compensated by adjusting the potential applied to $V2$. Residual fields are detected by monitoring the drift of a light ion (e.g., He^+) normal to the grids. By introducing a long delay (about 3 μs) between the ionizing pulse $P3$ and the extraction pulse $P2$, the ion drift is manifested by loss of resolution in the arrival time of the ions at the detector or by loss of ions due to migration out of the extraction volume. Either case leads to a reduction in the detected ion signal. Tuning the $V2$ grid voltage to maximize ion signal ensures a potential gradient across the excitation volume of less than 200 mV. The most uniform field was obtained when $V2$ was reduced by 4.8 V relative to $V1$ at 1500 V. These conditions were independently confirmed by a SIMION calculation [33].

The energy scale was calibrated by scanning over the threshold regions for He^+, Ne^+, and Ar^+ and shifting the energy scale to coincide with the photoionization threshold energy [34]. This procedure was supplemented by recording the ratios of ionization for different rare gases [i.e., $I(He^+)/I(Ar^+), I(Ne^+)/I(Ar^+)$, and $I(Ar^+)/I(Kr^+)$] and comparing them to the reference data of SHM and WBHF. This check was necessary because the determination of σ in the threshold region by Eq. (1) is sensitive to energy shifts in both the measured data and the reference data. The energy correction varies by less than ± 0.3 eV on a day-to-day basis. The adjusted absolute energy scale is accurate to about 0.5 eV.

6. Estimation of errors

The sources of error in determining cross sections by Eq. (1) are the accuracy of measuring ion intensities, the quality of the reference cross sections $\sigma_R(E)$, and the instrumental effects encompassed by $\kappa_{M,R}$ in Eq. (2). The signal-to-noise ratio in making analog measurements is much greater than 100, and the reproducibility in recording energy-dependent ion yield curves is about 1%. The reference cross section data for Ar^+ were derived from four different sets of measurements (Sec. II B 1). All of the individual measurements agree to within 10% of the reference values and to within 5% for energies above the threshold region.

The instrumental effects are separated into three components [Eq. (2)]. The correction term Γ_{defl} for the m/z deflection efficiency deviates from unity by no more than 1.4% in all cases and this deviation is probably accurate to less than 0.5% (Sec. II B 2). The analog measurements are placed on an absolute intensity scale using the results of pulse counting experiments to overcome the dependence of detector efficiency on m/z. The accuracy of the correction term Γ_{det} for each charge is limited by counting statistics to less than 4%. This uncertainty cascades in the product of ratios needed to determine cross sections of higher charge reaching a maximum value of 17% for $n=6$. The most serious instrumental effect by our technique is normally due to focusing of the heavier masses along the molecular beam centerline (Sec. II B 4). This effect causes Γ_{nrel} to deviate from unity by 6.8% for Kr and 12.5% for Xe. We avoid dealing with this uncertainty by scaling our energy-dependent cross sections for

Kr^+ and Xe^+ to values reported by SHM and WBHF (Sec. II B 4). This provides us with reference cross sections for these ions to 470 eV with an uncertainty that is perhaps 2% greater than that of the Ar^+ reference data set in Table I.

The cumulative uncertainties affect the shape and absolute cross sections differently. Our measurements should introduce no more than a 2–4% uncertainty in the energy-dependent shape of the cross section other than the uncertainties that exist in the reference data described above. The absolute scale is expected to be less accurate. Estimated uncertainties are 8–12% for $n = 2$ increasing to 20–25% for $n = 6$ (the upper range is for the high-energy region).

III. RESULTS AND DISCUSSION

A. Cross sections

The partial ionization cross sections for Kr and Xe are plotted in Figs. 7–10 and compiled in Tables II and III. Also included in Figs. 7–10 are data by SHM [3,4], WBHF [5], and KS [6], which are arguably the most reliable measurements with which to compare. (These investigators compare their work to earlier results.) These previous experiments have achieved a level of refinement sufficient to give agreement in the shape of the cross section curves to within 10% and typically 5% away from threshold regions. We also cite MSB [7] and Nagy, Skutlartz, and Schmidt [22] for obtaining energy-dependent shapes for partial cross sections that are consistent with the results cited above. Other investigators have obtained good agreement with these studies for the rare gases, but not over an extensive range of energy and ion charge [9,10,35,36]. We limit our comparison to what we judge to be the most extensive and reliable measurements.

Modern investigations have been less successful in obtaining consistent agreement in the absolute value of multiple ionization cross sections. Whereas single-ionization cross sections now agree to within 5–10%, discrepancies for multiply charged ions in these same studies vary by

FIG. 8. Cross sections for $Kr + e \rightarrow Kr^{n+} + (n+1)e$ for $n = 4-6.$ $\cdots \cdot$, present data; $\circ$, KS data. The KS data were multiplied by 0.50 to obtain overlap with the present results.

FIG. 9. Cross sections for $Xe + e \rightarrow Xe^{n+} + (n+1)e$ for $n = 1-3.$ $\cdots \cdot$, present data; ——, SHM data; — — —, WBHF data.

FIG. 7. Cross sections for $Kr + e \rightarrow Kr^{n+} + (n+1)e$ for $n = 1-3.$ $\cdots \cdot$, present data; ——, SHM data; — — —, WBHF data.
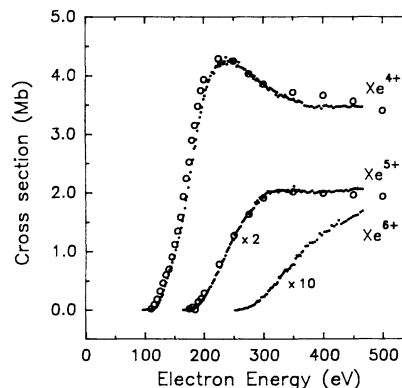
FIG. 10. Cross sections for $Xe + e \rightarrow Xe^{n+} + (n+1)e$ for $n = 4-6.$ $\cdots \cdot$, present data; $\circ$ KS data. The KS data were multiplied by 0.65 to obtain overlap with the present results.
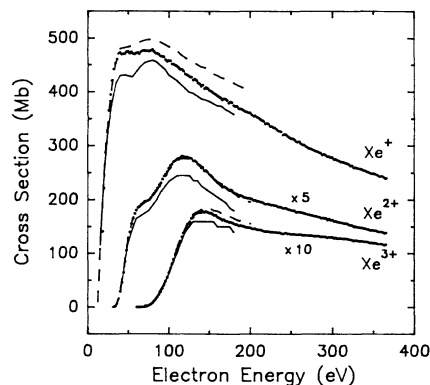
up to a factor of 2 [3–7]. The multiple-ionization cross sections reported here and in the work cited above were obtained by measuring relative ion abundances for different ion charges and scaling the values to cross sections for single ionization. The measurements of relative intensities for different ion charges are vulnerable to detector gain effects because ion impact energies depend directly on ion charge. This discrimination effect is acute for current mode detection, because the measured intensity ratios are in error by the gain factors (e.g., Fig. 5). Errors can also occur in pulse counting experiments because the PHD's depend strongly on gain as shown in Fig. 6. This problem has been discussed previously for Ar^{n+} studies [13]; however, we also show that it affects previ-

ously reported data for Kr^{n+} and Xe^{n+} multiple ionization.

We compare representative results of SHM, WBHF, and KS to the present measurements in Figs. 7–10. A more complete comparison of relative cross sections by different investigators is given in Tables IV and V. SHM and WBHF measured cross sections up to $n = 3$ for Kr^{n+} and Xe^{n+} (SHM also measured Kr^{4+}) and these are included in Figs. 7 and 9. Our results are in very good agreement with these data in both shape and magnitude (the greatest deviations at any energy are about 10%). KS measured cross sections to higher energy (1000 eV) and charge (Kr^{4+}, Xe^{5+}) than SHM and WBHF. We plot their data for $n \geq 4$ in Figs. 8 and 10. Excellent

TABLE II. Partial cross sections for electron-impact ionization to multiply charged ions of Kr (1 Mb$= 10^{-18}$ cm^2). Error limits are discussed in Sec. II B 6.

E (eV)	σ (10^{-18} cm^2)						E (eV)	σ(10^{-18} cm^2)					
	Kr^+	Kr^{2+}	Kr^{3+}	Kr^{4+}	Kr^{5+}	Kr^{6+}		Kr^+	Kr^{2+}	Kr^{3+}	Kr^{4+}	Kr^{5+}	Kr^{6+}
18	56.9						148	342	29.3	2.05	0.0036		
20	109						152	337	28.7	2.12	0.0064		
22	147						156	335	28.5	2.22	0.0102		
24	180						160	334	28.2	2.29	0.0154		
26	215						164	331	27.6	2.32	0.0217		
28	241						168	332	27.6	2.42	0.0288		
30	268						172	328	27.1	2.45	0.0355		
32	289						176	326	26.7	2.49	0.0412		
34	308	0.016					180	321	26.1	2.52	0.0467		
36	318	0.048					184	322	26.0	2.57	0.0552		
38	330	0.177					188	316	25.4	2.60	0.0631		
40	341	0.507					192	315	25.2	2.63	0.0748		
42	343	1.11					196	310	24.7	2.66	0.0834		
44	352	2.09					200	309	24.4	2.68	0.0915		
46	361	3.52					210	304	23.9	2.79	0.115	0.0008	
48	364	5.35					220	297	23.1	2.87	0.140	0.0012	
50	367	7.45					230	291	22.5	2.95	0.174	0.0025	
52	368	9.71					240	282	21.6	2.97	0.208	0.0047	
56	370	14.1					250	274	20.7	3.00	0.241	0.0070	
60	367	17.8					260	270	20.3	3.07	0.273	0.0124	
64	369	21.2					270	263	19.7	3.11	0.293	0.0148	
68	371	23.8					280	257	19.2	3.15	0.323	0.0185	
72	370	25.8					290	251	18.5	3.17	0.351	0.0236	
76	370	27.5	0.004				300	247	18.2	3.25	0.382	0.0277	
80	371	28.9	0.028				310	242	17.7	3.27	0.416	0.0347	
84	371	30.1	0.089				320	238	17.3	3.30	0.442	0.0404	0.0002
88	367	30.7	0.180				330	233	16.9	3.33	0.459	0.0494	0.0003
92	364	31.1	0.292				340	228	16.4	3.34	0.489	0.0552	0.0005
96	362	31.5	0.435				350	225	16.0	3.37	0.509	0.0639	0.0006
100	363	31.8	0.581				360	220	15.7	3.36	0.530	0.0675	0.0011
104	360	31.8	0.726				370	215	15.1	3.35	0.531	0.0735	0.0010
108	360	31.9	0.889				380	211	14.8	3.34	0.549	0.0816	0.0021
112	361	32.1	1.05				390	208	14.6	3.36	0.560	0.0911	0.0021
116	355	31.6	1.17				400	206	14.2	3.36	0.569	0.0955	0.0029
120	353	31.3	1.32				410	204	14.1	3.40	0.581	0.103	0.0035
124	353	31.2	1.45				420	200	13.8	3.39	0.590	0.109	0.0048
128	352	30.9	1.58				430	197	13.5	3.39	0.591	0.111	0.0052
132	353	30.9	1.68	0.0002			440	195	13.4	3.41	0.614	0.118	0.0064
136	347	30.3	1.79	0.0003			450	192	13.1	3.39	0.614	0.128	0.0073
140	345	29.9	1.89	0.0013			460	189	12.9	3.40	0.616	0.128	0.0074
144	342	29.6	1.97	0.0022			466	187	12.8	3.40	0.616	0.131	0.0085

agreement in shape (within 5%) is evident compared to our data; however, a large discrepancy exists in absolute magnitude. In order to obtain overlap with the present results, the data of KS were multiplied by factors of 0.50 (Kr^{4+}) and 0.65 (Xe^{4+}, Xe^{5+}). A discrepancy is also evident for the $n = 2$ and 3 cross sections of KS compared to those of SHM, WBHF, and here (Tables IV and V).

In a recent Letter, we reported multiple ionization cross sections for Ar and discussed the discrepancies that exist among recent measurements [13]. The strong dependence of MCP gain on ion-impact energy and, therefore, on ion charge can lead to systematic error in pulse counting measurements of relative intensity. This is illustrated in Fig. 11 for the intensity ratio for $I(Kr^{5+})/I(Kr^+)$ and $I(Xe^{3+})/I(Xe^+)$ as a function of discriminator level. The proper value of the cross section

ratio $\sigma_{Kr^{n+}}/\sigma_{Kr^+}$ is obtained only for low discriminator levels where the counting efficiency is the same for both ions. As discriminator levels are increased, the count rate for Kr^+ falls off more rapidly than for Kr^{n+} causing a distortion in the measure of relative cross section. The severity of this distortion increases with charge and, thus, overstates the cross section for multiple ionization. Ma, Sporleder, and Bonham [7] reported cross sections for Ar (but no other rare gas) that are in agreement with KS [6], but which differ from the results of SHM [3,4] and WBHF [5]. Our measurements of Ar [13], Kr, and Xe agree with the latter researchers.

The results of SHM employed a Faraday cup and electrometer to measure ion signal. This device measures total charge reaching the detector and is free of discrimination effects that depend on ion-impact energy. WBHF

TABLE III. Partial cross sections for electron-impact ionization to multiply charged ions of Xe. ($1 \text{ Mb} = 10^{-18} \text{ cm}^2$). Error limits are discussed in Sec. II B 6.

E (eV)	Xe^+	Xe^{2+}	Xe^{3+}	Xe^{4+}	Xe^{5+}	Xe^{6+}	E (eV)	Xe^+	Xe^{2+}	Xe^{3+}	Xe^{4+}	Xe^{5+}	Xe^{6+}
	σ (10^{-18} cm^2)							σ (10^{-18} cm^2)					
18	142						140	410	51.8	17.7	0.622		
20	222						144	406	50.7	17.7	0.746		
22	289						148	406	50.2	17.7	0.879		
24	328						152	402	48.8	17.6	1.03		
26	366						156	397	47.5	17.2	1.17		
28	396						160	393	46.4	16.8	1.32		
30	421						164	389	45.4	16.5	1.52		
32	442	0.12					168	388	45.0	16.4	1.74	0.0008	
34	454	0.48					172	384	44.2	16.0	1.94	0.0032	
36	461	1.45					176	382	43.8	15.8	2.23	0.0074	
38	472	3.23					180	375	42.7	15.6	2.50	0.0117	
40	473	5.83					184	374	42.2	15.4	2.76	0.0264	
42	469	9.19					188	368	41.7	15.2	2.92	0.0392	
44	470	13.0					192	365	40.9	15.1	3.20	0.0655	
46	471	17.1					196	363	40.6	14.9	3.38	0.0929	
48	475	21.2					200	361	40.5	14.8	3.60	0.120	
50	476	25.0					210	351	39.5	14.4	3.93	0.205	
52	471	28.0					220	342	38.5	14.2	4.14	0.317	
56	471	33.2					230	333	37.8	14.0	4.26	0.427	
60	472	36.2					240	320	36.8	13.7	4.19	0.538	
64	471	37.7	0.011				250	313	36.1	13.6	4.22	0.647	0.0004
68	477	38.8	0.042				260	308	35.6	13.6	4.23	0.718	0.0012
72	476	39.6	0.160				270	296	34.5	13.3	4.11	0.827	0.0036
76	476	40.2	0.417				280	290	33.9	13.3	3.99	0.865	0.0092
80	479	41.8	0.873				290	285	33.2	13.1	3.95	0.917	0.0148
84	472	43.4	1.56				300	278	32.6	13.1	3.88	0.965	0.0240
88	470	45.6	2.43				310	270	31.5	12.8	3.75	0.993	0.0386
92	466	47.8	3.53				320	266	30.7	12.6	3.73	1.02	0.0442
96	460	49.5	4.91				330	258	29.8	12.4	3.67	1.03	0.0621
100	459	51.9	6.48				340	254	29.2	12.1	3.64	1.03	0.0708
104	452	53.3	8.12	0.005			350	248	28.5	11.9	3.60	1.06	0.0783
108	449	54.7	9.82	0.008			360	244	28.1	11.8	3.58	1.01	0.0923
112	445	55.5	11.6	0.014			370				3.48	1.01	0.110
116	442	56.3	13.1	0.029			390				3.46	1.00	0.121
120	433	55.7	14.4	0.065			410				3.47	1.02	0.136
124	430	55.6	15.6	0.134			430				3.47	1.02	0.147
128	427	55.3	16.6	0.231			450				3.50	1.03	0.161
132	424	54.6	17.4	0.349			466				3.47	1.03	0.170
136	417	53.1	17.7	0.477									

TABLE IV. Ratios of partial cross sections for multiple ionization of Kr.

$M(n,m)$	E	$\sigma(M^{n+})/\sigma(M^{m+})$			
		This work	SHM[a]	WBHF[b]	KS[c]
Kr(2,1)	50	0.020 3	0.028	0.021	0.019 9
	100	0.087 7	0.087	0.086 0	0.097 0
	150	0.085 6	0.087	0.082 6	0.092 7
	200	0.079 2		0.076 6	0.085 2
Kr(3,1)	100	0.001 60	0.001 8	0.001 9	0.002 99
	150	0.006 20	0.006 5	0.007 0	0.010 9
	200	0.008 68		0.010 1	0.015 7
	300	0.013 2			0.022 6
Kr(4,1)	150	0.000 02	0.000 03		0.000 05
	180	0.000 15	0.000 30		0.000 33
	300	0.001 55			0.003 18
	400	0.002 76			0.005 92

[a]Reference [3].
[b]Reference [5].
[c]Reference [6].

used a MCP and pulse counting to measure ion intensities. They investigated the gain characteristics of their detector and the experimental conditions (gain saturation, discriminator levels) that ensure maximum counting efficiency for all ions. The present experiment has also established valid pulse counting conditions so that detector gain effects with ion charge state are minimal (Sec. II B 3 and Fig. 11). The agreement of our measurements with SHM and WBHF for which gain effects are either absent or avoided gives us confidence in the absolute cross-section values reported here. It is difficult to judge whether the KS results suffer from detector-gain effects

TABLE V. Ratios of partial cross sections for multiple ionization of Xe.

$M(n,m)$	E	$\sigma(M^{n+})/\sigma(M^{m+})$			
		This work	SHM[a]	WBHF[b]	KS[c]
Xe(2,1)	50	0.052 6	0.055	0.0537	0.069 0
	100	0.113	0.108	0.105	0.120
	150	0.122	0.113	0.113	0.119
	200	0.112		0.097 0	0.102
Xe(3,1)	100	0.014 1	0.015	0.013	0.021 8
	150	0.043 7	0.041	0.0428	0.060 2
	200	0.041 1		0.038 7	0.054 3
Xe(4,1)	150	0.002 33	0.002 3		0.004 47
	200	0.009 97			0.017 6
	300	0.013 9			0.021 0
Xe(5,1)	200	0.000 33			0.000 65
	300	0.003 47			0.005 21
	400	0.004 55			0.006 38

[a]Reference [4].
[b]Reference [5].
[c]Reference [6].
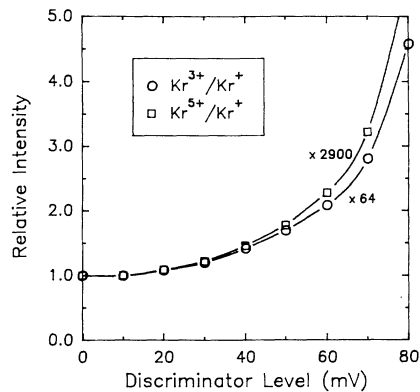

FIG. 11. Ratio of ion counts for $I(Kr^{3+})/I(Kr^{+})$ and $I(Kr^{5+})/I(Kr^{+})$ as a function of discriminator level. Electron energy was 370 eV.

because sufficient experimental detail is not provided. These investigators employ pulse counting but the detector used is not mentioned; we assume an electron multiplier from their earlier work [37]. The increased discrepancy in their measured cross sections with increasing n is consistent with a detector gain effect. As mentioned in Sec. II B 3, the gain-effect problem is reduced by working close to gain-saturation conditions.

B. Threshold measurements

Threshold energies for ionization (which we loosely call ionization potentials) are presented in Table VI and compared to previous determinations. Ionization potentials are not reported in the most recent measurements of multiple-ionization cross sections [3–7] except for WBHF [5], who report values up to $n = 3$ for Kr^{n+} and Xe^{n+}. The nature of these recent experiments demands some sacrifice of sensitivity and dynamic range in order to improve the accuracy of measuring cross sections. For example, gas density is minimized to avoid ion-neutral collisions and ion production rates are reduced to achieve valid pulse counting statistics. Our experiment achieves greater sensitivity because of the use of high-density gas pulses and gated analog detection to record the cross-section energy dependence. Pulse counting is employed at just a few energies to normalize the analog curves. Our sensitivity though is limited by our choice of a hairpin filament that offers good energy resolution but low electron flux. Previous reports of ionization potentials for multiply charged ions are mainly based on commercial mass spectrometers designed for detection sensitivity and not cross-section measurements.

Simple theory predicts that the threshold ionization probability $P(E)$ should obey a power law of the form $P(E)=c(E-E_0)^n$, where c is a scaling constant, E_0 is the ionization potential, and n is the number of electron degrees of freedom (taken to be the number of ionized electrons) [23,38]. Other studies have recognized that the threshold regions are often composed of a series of segments that appear as breaks in the curves [16,17,39]. The threshold law successfully describes results for singly and

TABLE VI. Multiple-ionization potentials by electron impact.

M^{n+}	n	Ionization potential (eV)							
		This work[a]	WBHF[b]	Stuber[c]	Fox[d]	DMN[e]	TS[f]	Bleakney[g]	Spectroscopy[h]
Ar	3	84 (81)		85	84.8	83.7		88	84.13
	4	148 (135)		147	150.0			258	143.9
	5	225		285					218.9
Kr	3	74 (72)	62.9	76	75.6		77		75.31
	4	130 (127)		134	147		145		~145
	5	195		204	218				
	6	280		302	350				
Xe	3	64 (61)	62.9	65		64.8	66		65.46
	4	104 (100)		110		107	112		~111
	5	166 (163)		172		160	188		~187
	6	230		248		218	275		

[a]The Ar cross sections are from Ref. [13]. E_0 values were determined by fitting $\sigma(E)$ to $P(E)=c(E-E_0)^{1/n}$ where c, E_0, and n are fitting parameters. Values in parentheses were determined from linear fits of $\sigma^{1/n}$ for fixed n. When only one value appears, E_0 was estimated by extrapolating σ curves to zero.

[b]Reference [5].
[c]Reference [17].
[d]Reference [16].
[e]Reference [18].

[f]Reference [15].
[g]Reference [14].
[h]References [34] and [41].

doubly charged rare-gas ions and extrapolates very close to spectroscopic ionization potentials [5,16,19]. Attempts to extract E_0 for higher charged ions from linearized plots of $P(E)^{1/n}$ have shown only moderate success. Fox found that the n-power law leads to values of E_0 less than the spectroscopic values [16]. WBHF report that Kr^{2+} and Xe^{2+} rise quadratically, but only Kr^{3+} and not Xe^{3+} rose cubically, although poor signal-to-noise could be to blame [5]. Regardless, their E_0 values for the triply charged ions are significantly less than the spectroscopic values (Table VI).

The data measured here were fitted in the threshold region to the power-law function $P(E)$ for σ and to a linearized function of $\sigma^{1/n}$. This analysis was used to determine E_0 as shown by the examples in Figs. 12 and

13 for Kr^{3+} and Xe^{5+}. Values of E_0 obtained by both fitting routines are reported in Table VI (an analysis of our previously published Ar^{n+} data is also included [13]). In some cases, the signal-to-noise ratio was inadequate to obtain a reliable fit, in which case E_0 was estimated by manual extrapolation of σ to zero. The σ and $\sigma^{1/n}$ plots are extremely sensitive to baseline shifts and scatter in the data, especially as n increases. Baseline effects were corrected by subtracting from our cross-section curves the average baseline value preceding E_0. The linear extrapolations give E_0 values that are always lower than those obtained directly from fitting σ plots (Table VI and Figs. 12 and 13). Since the latter determination gives good agreement with the few available spectroscopic values [34], we assume that these values are the more reli-
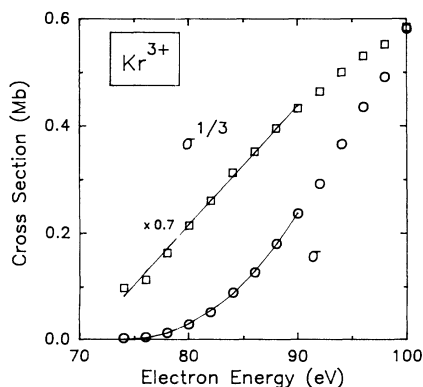

FIG. 12. Threshold cross sections for Kr^{3+} production. The fitting parameters for the power-law expression to σ are $E_0=74$ and $n=2.14$. The units of $\sigma^{1/3}$ are $Mb^{1/3}$.
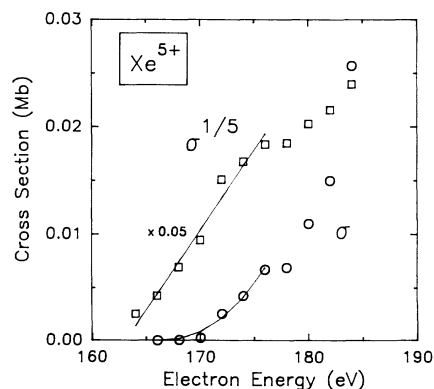

FIG. 13. Threshold cross sections for Xe^{5+} production. The fitting parameters for the power law expression to σ are $E_0=166$ and $n=2.32$. The units for $\sigma^{1/5}$ are $Mb^{1/5}$.

able. Our values of E_0 are consistently less than those reported by Fox [16] and Stuber [17] and in better agreement with spectroscopic values. Our measurements of E_0 for multiply charged Ar, Kr, and Xe are, therefore, believed to be significant improvements over existing values. This is especially important for Kr and Xe, for which spectroscopic data is not available above $n = 3$. Dorman, Morrison, and Nicholson (DMN) [18] measured values for Xe^{n+} that are similar to (and in some cases less than) our values (Table VI). We have no reason to judge their values any less reliable than ours.

The measure of ionization thresholds was not the primary intent of this work. The threshold data used to determine E_0 values (e.g., Figs. 12 and 13) were taken from full cross-section curves and were not optimized for weak signal. There are a few experimental and procedural modifications that would significantly improve on the reported values, of which we mention two. First, pulse counting is preferable to analog detection for measuring weak signal (and would eliminate baseline effects). In the future we intend to use pulse counting for all threshold measurements instead of analog measurements normalized to pulse-counting results obtained at a few energies. Second, a pulsed deflection field near the detector would be useful for preventing strong signals from affecting the baseline of very weak signals of interest.

IV. SUMMARY AND CONCLUSIONS

Great progress has been made in the past decade toward improving the methods for measuring electron-impact-ionization cross sections. Commercial quadrupole mass spectrometers have for the most part been abandoned in favor of devices that allow field-free ionization and uniform collection efficiency for all masses of interest. Independent measurements of cross sections for single ionization are now in close agreement. There still remains a problem in measuring multiple-ionization cross sections, where large discrepancies among recent studies suggest the presence of instrumental effects that discriminate on the basis of ion charge.

In this work we report on multiple ionization of Kr and Xe, which follows our previous work on Ar [13]. Partial cross sections were measured for the ionization $M + e \rightarrow M^{n+} + (n+1)e$ for $M = $ Kr and Xe ($n = 1-6$) as a function of electron energy (0–470 eV). Cross-section values are reported for previously unmeasured Kr^{5+}, Kr^{6+}, and Xe^{6+}. The cross sections reported for the remaining ions considerably narrow the uncertainty of past measurements. The experiments make use of

crossed electron and atomic beams, time-of-flight mass spectrometry, pulsed beam sources, and pulsed ion extraction. The method offers field-free ionization and narrow energy resolution, uniform collection efficiency as a function of m/z, and simultaneous detection of more than one ion signal. Particular attention is given to the issue of electron-multiplier gain dependence on ion-impact energy. Because impact energy varies with ion charge, the measure of relative intensities for ions of different charge are vulnerable to gain discrimination effects. It is commonly believed that pulse counting alleviates gain discrimination effects. We recorded pulse-height distributions for different ion charges to show that this is true only if discriminator levels are properly set.

The present technique has excellent sensitivity compared to other methods that offer reliable energy-dependent cross sections. Further improvements are possible which will aid in measuring ionization threshold regions and cross sections for higher ion charges. We recently tested a scheme whereby pulsed excitation and TOF mass spectra are triggered repetitively over the duration of a single gas pulse. This raises the effective repetition rate from 50 to about 500 Hz [40]. Our technique may have its greatest utility in measuring dissociative ionization of molecules. The supersonic expansion considerably cools the rovibrational distribution permitting better energy resolution. In addition, the pulsed extraction and high-energy ion acceleration minimizes losses in detection efficiency due to fragment kinetic energy [40].

After submission of this paper, two new studies were reported that bolster the conclusions reached in this paper. Tarnovsky and Becker measured the cross section ratios for $\sigma(Ar^{2+})/\sigma(Ar^+)$ and $\sigma(Kr^{2+})/\sigma(Kr^+)$ by the fast-atom-beam techniques and report values of 0.066 ± 0.007 and 0.087 ± 0.008, respectively, at 100 eV [42], which is in excellent agreement with our values of 0.0625 [13] and 0.0877 (Table IV). These authors also mention that Bonham and collaborators remeasured their value for $\sigma(Ar^{2+})/\sigma(Ar^+)$ at 100 eV and obtained 0.073 ± 0.006 [43] (down from 0.087 [7]), which is in much better agreement with the emerging consensus of values [13].

ACKNOWLEDGMENTS

[1] Electron Impact Ionization, edited by T. D. Märk and G. H. Dunn (Springer-Verlag, New York, 1985).

[2] L. J. Kieffer and G. H. Dunn, Rev. Mod. Phys. **38**, 1 (1966).

[3] K. Stephan, H. Helm, and T. D. Märk, J. Chem. Phys. **73**, 3763 (1980).

[4] K. Stephan and T. A. Märk, J. Chem. Phys. **81**, 3116 (1984).

[5] R. C. Wetzel, F. A. Baiocchi, T. R. Hayes, and R. S.

Freund, Phys. Rev. A **35**, 559 (1987).

[6] E. Krishnakumar and S. K. Srivastava, J. Phys. B **21**, 1055 (1988).

[7] C. Ma, C. R. Sporleder, and R. A. Bonham, Rev. Sci. Instrum. **62**, 909 (1991).

[8] D. Rapp and E. Englander-Golden, J. Chem. Phys. **43**, 1464 (1965).

[9] A. Crowe, J. A. Preston, and J. W. McConkey, J. Chem. Phys. **57**, 1620 (1972).

[10] D. Mathur and C. Badrinathan, Int. J. Mass Spectrom. Ion Proc. **57**, 167 (1984).

[11] R. S. Freund, R. C. Wetzel, R. J. Shul, and T. R. Hayes, Phys. Rev. A **41**, 3575 (1990); R. S. Freund, R. C. Wetzel, and R. J. Shul, *ibid.* **41**, 5861 (1990).

[12] J. A. Syage, Chem. Phys. Lett. **143**, 19 (1988).

[13] J. A. Syage, J. Phys. B **24**, L527 (1991).

[14] W. Bleakney, Phys. Rev. **36**, 1303 (1930).

[15] J. T. Tate and P. T. Smith, Phys. Rev. **46**, 773 (1934).

[16] R. E. Fox, J. Chem. Phys. **33**, 200 (1960).

[17] F. A. Stuber, J. Chem. Phys. **42**, 2639 (1965).

[18] F. H. Dorman, J. D. Morrison, and A. J. C. Nicholson, J. Chem. Phys. **31**, 1335 (1959).

[19] J. D. Morrison and A. J. C. Nicholson, J. Chem. Phys. **31**, 1320 (1959).

[20] B. L. Schram, F. J. De Heer, M. J. Van der Wiel, and J. Kistemaker, Physica **31**, 94 (1965); B. L. Schram, J. H. Boerboom, and J. Kistemaker, *ibid.* **32**, 185 (1966); B. L. Schram, *ibid.* **32**, 197 (1965).

[21] M. J. Van der Wiel, Th. M. El-Sherbini, and L. Vriens, Physica **42**, 411 (1969); Th. M. El-Sherbini, M. J. Van der Wiel, and F. J. De Heer, *ibid.* **48**, 157 (1969).

[22] P. Nagy, A. Skutlartz, and V. Schmidt, J. Phys. B **13**, 1249 (1980).

[23] E. P. Wigner, Phys. Rev. **73**, 1002 (1948); G. H. Wannier, *ibid.* **90**, 817 (1953); **100**, 1180 (1956).

[24] By partial cross section, we mean ionization to specific final charge summed over all states.

[25] J. A. Syage, J. Chem. Phys. **92**, 1804 (1990); J. A. Syage and J. Steadman, Rev. Sci. Instrum. **61**, 1204 (1990); J. A. Syage, J. E. Pollard, and J. Steadman, Chem. Phys. Lett. **161**, 103 (1989).

[26] J. A. Syage, J. Phys. Chem. **93**, 170 (1989); J. A. Syage, J. E. Pollard, and R. B. Cohen, Appl. Opt. **26**, 3516 (1987).

[27] J. A. Syage and J. Steadman, J. Chem. Phys. **95**, 2497 (1991); J. Steadman and J. A. Syage, J. Am. Chem. Soc. **113**, 6786 (1991).

[28] J. E. Pollard and R. B. Cohen, Rev. Sci. Instrum. **58**, 32 (1987).

[29] C. LaLau, in *Advances in Analytical Chemistry and Instrumentation, Vol. 8,* edited by A. L. Burlingame (Wiley, Newark, 1970), p. 93; C. N. Burrous, A. J. Lieber, and V. T. Zaviantseff, Rev. Sci. Instrum. **38**, 1477 (1967).

[30] S. A. Fields, J. L. Burch, and W. A. Oran, Rev. Sci. Instrum. **48**, 1076 (1977); J. N. Fox, R. L. Fitzwilson, and E. W. Thomas, J. Phys. E **3**, 36 (1970).

[31] J. L. Wiza, Nucl. Instrum. Methods **162**, 587 (1979).

[32] J. B. Anderson, R. P. Andres, and J. B. Fenn, Adv. Chem. Phys. **10**, 275 (1966); A. Kantrowitz and J. Grey, Rev. Sci. Instrum. **22**, 328 (1951).

[33] D. A. Dahl and J. E. Delmore, The Simion PC/PS2 User's Manual, Ver 4.0 EG&G Idaho National Engineering Laboratory Report No. EGG-CS-7233, Rev. 2, 1988 (unpublished).

[34] D. D. Wagman, W. H. Evans, V. B. Parker, R. H. Schumm, I. Halow, S. M. Bailey, K. L. Churney, and R. L. Nuttall, The NBS Tables of Chemical Thermodynamic Properties, J. Phys. Chem. Rev. Data. Suppl. No. 2 (American Institute of Physics, New York, 1982), Vol. 11, pp. 2–41ff.

[35] D. Mathur and C. Badrinathan, Int. J. Mass. Spectrum. Ion Proc. **68**, 9 (1986).

[36] J. Fletcher and I. R. Cowling, J. Phys. B **6**, L258 (1973).

[37] O. J. Orient and S. K. Srivastava, J. Chem. Phys. **78**, 2949 (1983).

[38] J. D. Morrison and J. C. Traeger, J. Chem. Phys. **53**, 4053 (1970).

[39] R. E. Winters, J. H. Collins, and W. L. Courchene, J. Chem. Phys. **45**, 1931 (1966).

[40] J. A. Syage, J. Chem. Phys. **97**, 6085 (1992).

[41] G. Herzberg, *Atomic Spectra and Atomic Structure* (Dover, New York, 1944), pp. 200 and 201.

[42] V. Tarnovsky and K. Becker, Z. Phys. D **22**, 603 (1992).

[43] Cited as Ref. 24 in Ref. [42].